PCCP

ROYAL SOCIETY OF CHEMISTRY

PAPER

View Article Online
View Journal | View Issue

Check for updates

Cite this: *Phys. Chem. Chem. Phys.*, 2026, **28**, 271

Covalent bonding and extreme shielding in xenon–icosagen fluoride cations

Erick Cerpa, *[a] Jose A. Guerrero-Cruz, [b] Gabriel Merino, [c] J. Oscar C. Jimenez-Halla [d] and Abril C. Castro *[b]

Received 3rd September 2025,
Accepted 12th November 2025

DOI: 10.1039/d5cp03397g

rsc.li/pccp

Although icosagen cations are known to interact significantly with noble gases, well-defined examples exhibiting strong binding energies indicative of covalent character, particularly for the heavier icosagens, remain scarce. In this work, we explore the stability and bonding of a series of $XeMF_2^+$ and $Xe_2MF_2^+$ (M = B–Tl) cations, focusing on global-minimum structures featuring Xe–M bonds. *Ab initio* calculations indicate that these species are thermodynamically viable at 298 and 398 K, with all considered dissociation pathways being endergonic. Bonding analyses reveal strong covalent Xe–icosagen interactions for B, Al, and Ga, while In and Tl exhibit weaker bonding character that suggests more ionic interactions, as supported by the selected complementary analyses. Fluoride ion affinities and relativistic ^{129}Xe NMR chemical shifts further support the strong electron-withdrawing nature of the MF_2^+ cations. Overall, the results suggest that, beyond the previously reported $XeBF_2^+$, Xe–icosagen compounds such as $XeAlF_2^+$ and $XeGaF_2^+$ may also be experimentally accessible.

Open Access Article. Published on 01 December 2025. Downloaded on 5/2/2026 7:54:11 AM.
This article is licensed under a Creative Commons Attribution 3.0 Unported Licence.

Introduction

The synthesis, characterization, and theoretical prediction of noble-gas (Ng) compounds have long posed a scientific challenge. The long-held assumption of Ng chemical inertness was overturned in 1962,[1–3] and since then, Ng chemistry has evolved into a dynamic field of experimental and theoretical research.[4–8] While compounds of heavier Ngs such as Kr, Xe, and Rn can be stabilized under relatively mild conditions (despite the high radioactivity of Rn), those of He, Ne, and Ar require extreme conditions, such as cryogenic temperatures or very high pressures.[9,10] Most known Ng compounds involve halogen or oxygen, but a broader range of elements, including the icosagens (Group-13), can also form neutral or cationic species incorporating Ngs. This reactivity is often driven by a combination of suitable electronegativity and electron-donation capabilities.

In recent years, there has been growing interest in compounds featuring covalent Ng–B bonds.[11–24] Several boron-containing cations, such as $NgBF_2^+$,[25] $NgBH_4^+$,[21] $NgBH_2^+$, and $Ng_2BH_2^+$ (Ng = Ar–Rn),[26] have been reported as both thermodynamically and kinetically viable. In contrast, much less attention has been paid to species involving heavier icosagens. Only a few studies have examined E^+–Ng (E = Al–In) cations,[27,28] or the insertion of Ng atoms into B- and Al-containing fluorides[29] or hydroxides.[30] Donor–acceptor complexes, such as F_3Al–Ng–NH_3, have also been investigated,[31] revealing bonding scenarios that include covalent Ng–AlF_3 and electrostatic Ng–NH_3 contacts. Additionally, metastable Xe compounds of the type XXe–EX_2 (X = F–I; E = B–Ga) have been reported,[32] where the Xe–E bond retains a covalent character regardless of the halogen involved. These findings collectively highlight the potential of heavier icosagens to engage in bonding with noble gases, yet comprehensive studies in this area remain limited.

The ability of icosagens to form strong interactions with Ngs offers a promising route for designing novel, stable compounds with distinctive electronic and structural properties. Among these, Xe–icosagen compounds are particularly intriguing due to the unique electronic, magnetic, and structural features of Xe.[33] Xenon's large, polarizable electron cloud makes it highly sensitive to its chemical environment, a property that underlies its exceptional performance in nuclear magnetic resonance (NMR) spectroscopy. ^{129}Xe NMR chemical shifts span an unusually broad range of approximately 7500 ppm,[34] enabling it to serve as a powerful probe for detecting weak interactions.[35,36] Consequently, there is considerable interest in modeling and interpreting ^{129}Xe NMR chemical shifts, especially in systems where Xe engages in covalent or electrostatic bonding with other elements.[37–42]

[a] *Departamento de Formación Básica Disciplinaria, Unidad Profesional Interdisciplinaria de Ingeniería Campus Guanajuato, Instituto Politécnico Nacional, C.P. 36275, Silao de la Victoria, Gto, Mexico. E-mail: jcerpa@ipn.mx*
[b] *Hylleraas Centre for Quantum Molecular Sciences, Department of Chemistry, University of Oslo, 0315 Oslo, Norway. E-mail: abril.castro@kjemi.uio.no*
[c] *Departamento de Física Aplicada, Centro de Investigación y de Estudios Avanzados, Unidad Mérida, Km 6 Antigua Carretera a Progreso. Apdo. Postal 73, Cordemex, 97310, Mérida, Yuc, Mexico*
[d] *Departmento de Química, División de Ciencias Naturales y Exactas, Universidad de Guanajuato, Noria Alta s/n,, 36050, Guanajuato, Gto, Mexico*

Open Access Article. Published on 01 December 2025. Downloaded on 5/2/2026 7:54:11 AM.
This article is licensed under a Creative Commons Attribution 3.0 Unported Licence.

In this study, we examine the nature and strength of Xe–icosagen bonding in the cationic species $XeEF_2^+$ and $Xe_2EF_2^+$ (E = B–Tl). To evaluate their stability, we performed *ab initio* calculations of dissociation energies (D_e), enthalpies (ΔH), and Gibbs free energies (ΔG). We also employed various bonding descriptors to characterize the Xe–E interactions. Furthermore, we calculated fluoride ion affinities (FIA) and predicted ^{129}Xe NMR chemical shifts to gain deeper insight into the electronic environment in these complexes and to guide future experimental studies. Finally, we analyzed the impact of relativistic effects on the NMR shifts using both two-component ZORA and fully four-component DKS approaches.

Computational details

The potential energy surfaces of the $XeEF_2^+$ and $Xe_2EF_2^+$ (E = B–Tl) compounds were systematically explored using a modified genetic algorithm implemented in the Global Optimization of Molecular Systems (GLOMOS) program[43] at the PBE0/def2-TZVP[44,45] level. The lowest-energy structures were then reoptimized at the MP2 level using either the def2-TZVP or aug-cc-pVTZ basis sets. For Xe, In and Tl atoms, quasi-relativistic pseudopotentials were employed to account for core electrons.[46–48] Final single-point energies were computed at the CCSD(T)/def2-TZVP level, with zero-point energy corrections obtained from MP2/def2-TZVP frequencies. All quantum chemical calculations were performed using Gaussian 16.[49]

To probe the nature of the Xe–icosagen bonding, several complementary approaches were applied. Energy decomposition analysis (EDA)[50–52] was conducted at the BP86-D3(BJ)/TZ2P//MP2/def2-TZVP level,[53–56] using the zeroth-order regular approximation (ZORA) Hamiltonian to account for scalar relativistic effects,[57–61] as implemented in ADF.[62] Additional bonding analyses included adaptive natural density partitioning (AdNDP),[63,64] natural population analysis (NPA), and Wiberg bond indexes (WBI), all computed at the MP2/def2-TZVP level. To further probe bonding characteristics, we also evaluated non-covalent interactions (NCI),[65,66] the electron localization function (ELF),[67,68] and the localized-orbital locator (LOL).[69–72] These analyses were carried out using Multiwfn.[73] Full methodological details for EDA, AdNDP, ELF, and LOL are provided in the SI.

Fluoride ion affinities (FIA) were evaluated to further investigate the Lewis acidity of the EF_2^+ fragments in the $XeEF_2^+$ and $Xe_2EF_2^+$ cations. FIA values correspond to the negative enthalpy change ($-\Delta H$) of the following reaction:

$$A^+ + F^- \xrightarrow[FIA=-\Delta H]{\Delta H} AF$$

Enthalpies were obtained from geometry optimizations at the CCSD(T)/def2-TZVPP level. For the larger $B(C_6F_5)_2^+$ species, the ωB97X-D/def2-TZVPP level was employed instead, due to computational cost constraints.

Relativistic ^{129}Xe NMR chemical shifts were computed in the gas phase using the fully four-component Dirac–Kohn–Sham (4c-DKS) method with the Dirac–Coulomb Hamiltonian,[74,75] as implemented in the ReSpect program.[76] The hybrid PBE0 functional was combined with the uncontracted Dyall's VQZ[77–79] basis set. To evaluate the impact of relativistic effects, additional calculations were carried out using the scalar relativistic ZORA (SR-ZORA) and the two-component spin–orbit ZORA (SO-ZORA) approximations, both available in ADF. In these cases, the PBE0 functional was also used, together with the all-electron Slater-type QZ4P[80] basis set. All ^{129}Xe NMR chemical shifts are reported relative to $XeOF_4$. Gauge-origin dependence was handled using the gauge-including atomic orbitals (GIAO) approach.[75,81]

All computational data are available in the ioChem-BD repository[82] and can be accessed *via* **https://doi.org/10.19061/iochem-bd-6-567**.

Results and discussion

Structure and stability

The global and local minimum structures of the $XeEF_2^+$ and $Xe_2EF_2^+$ (E = B–Tl) compounds are summarized in Tables S1 and S2. We first focus on the $XeEF_2^+$ (**1a**) and $Xe_2EF_2^+$ (**2a**) systems with E = B–In; the Tl analogues are discussed separately, as they exhibit a distinct potential-energy surface topology. The global minima identified for the former species correspond to singlet states with C_{2v} symmetry, formed by the interaction of one or two Xe atoms with the EF_2^+ cation (Fig. 1). The **1a** species represent deep energy minima, with the next lowest isomers lying more than 50 kcal mol^{-1} higher in energy (Table S1). In contrast, **2a** species have a competitive C_{2v} planar form (**2b**) that is only slightly less stable by 2.0 (B), 16.1 (Al), 15.0 (Ga), and 13.4 (In) kcal mol^{-1}. Interestingly, **2b** arises from the insertion of a second Xe atom into the $XeEF_2^+$ (**1a**) fragment (Table S2).

Geometrical parameters for the **1a** and **2a** species are listed in Tables S4 and S5, respectively. At the MP2/def2-TZVP level, the Xe–B and B–F bond lengths in $XeBF_2^+$ are 2.274 and 1.272 Å, respectively, in excellent agreement with previously reported values of 2.278 and 1.273 Å at the MP2/aug-cc-pVTZ/SDD level.[25] Moreover, the Xe–E bond lengths in both **1a** and **2a** species closely match the sum of the covalent radii and are substantially shorter than those found in Xe–E$^+$ (E = Al–In) systems,[27,28] indicating a strong interaction between Xe and the EF_2^+ core. Comparison of the geometries of **1a** and **2a** reveals minor elongation in the Xe–E and E–F bonds in **2a**, suggesting that

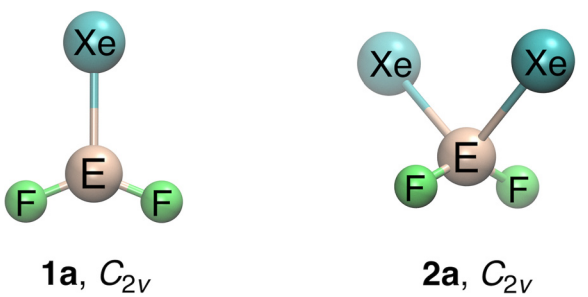

Fig. 1 Minimum-energy structures of the $XeEF_2^+$ (**1a**) and $Xe_2EF_2^+$ (**2a**) species (E = B–Tl) at the MP2/def2-TZVP level.

 This journal is © the Owner Societies 2026

Open Access Article. Published on 01 December 2025. Downloaded on 5/2/2026 7:54:11 AM.
This article is licensed under a Creative Commons Attribution 3.0 Unported Licence.

the addition of a second Xe atom does not significantly alter the electronic structure of **1a**.

The stability of $XeTlF_2^+$ and $Xe_2TlF_2^+$ differs slightly from that of the lighter congeners (Tables S1 and S2). After refinement of the relative energies at the CCSD(T)/def2-TZVP level, **1a** remains the global minimum for both species. However, additional low-lying isomers are identified. For $XeTlF_2^+$, a nearly isoenergetic linear $C_{\infty v}$ isomer (**1c**) lies only 0.3 kcal mol^{-1} above the global minimum (Table S1). Likewise, five local minima within 15.0 kcal mol^{-1} of the global minimum are found for $Xe_2TlF_2^+$ (Tables S2 and S3). These results indicate that Xe–Tl bonding is weaker than in the lighter analogues. High-spin structures were also considered but proved significantly less stable. The lowest-energy triplet structure lies 55.4 and 45.0 kcal mol^{-1} above **1a** and **2a**, respectively.

To evaluate the thermodynamic and kinetic stability of **1a** and **2a**, we calculated dissociation energies (D_e), enthalpies (ΔH), and Gibbs free energies (ΔG) at room temperature using the MP2/def2-TZVP level. Three dissociation channels were considered (where n = 1, 2):

$$Xe_nEF_2^+ \rightarrow nXe + EF_2^+ \quad (1)$$

$$Xe_nEF_2^+ \rightarrow Xe_nE^+ + F_2 \quad (2)$$

$$Xe_nEF_2^+ \rightarrow nXe + E^+ + F_2 \quad (3)$$

Among these three dissociation pathways, the one described in eqn (1) is the most favorable for both **1a** and **2a** (Table 1). This process is endothermic and endergonic, with dissociation being more endothermic for **2a** than for **1a**. In contrast, the other two channels, loss of F_2 (eqn (2)) and full fragmentation into Xe, E^+, and F_2 (eqn (3)), require significantly more energy.

Table 1 Dissociation energies (D_e), enthalpies (ΔH), and Gibbs free energies (ΔG) for $XeEF_2^+$ (**1a**) and $Xe_2EF_2^+$ (**2a**) species computed at the MP2/def2-TZVP level. All values are expressed in kcal mol^{-1}

	$XeEF_2^+$ (**1a**)			$Xe_2EF_2^+$ (**2a**)		
M	D_e[a]	ΔH	ΔG[b]	D_e[a]	ΔH	ΔG[b]
(1)	$Xe_nEF_2^+ \rightarrow nXe + EF_2^+$					
B	24.9 (25.7)	25.0	19.1	30.6 (30.2)	30.8	18.6
Al	28.2 (29.0)	28.2	22.6	46.4 (47.0)	46.1	33.5
Ga	24.5 (25.1)	24.6	19.2	41.8 (42.1)	41.6	29.7
In	19.0 (18.5)	19.0	14.4	34.7 (33.4)	34.5	23.3
Tl	13.9 (12.8)	14.0	9.1	26.5 (24.1)	26.3	15.6
(2)	$Xe_nEF_2^+ \rightarrow Xe_nE^+ + F_2$					
B	270.0 (252.7)	266.8	257.5	265.4 (248.3)	262.3	251.9
Al	201.9 (189.5)	200.5	192.0	214.5 (202.4)	212.8	201.9
Ga	134.9 (123.3)	133.9	125.1	146.1 (134.9)	144.9	134.1
In	88.8 (83.0)	88.1	80.1	99.0 (93.3)	98.0	88.0
Tl	30.7 (30.3)	30.0	21.6	37.2 (36.8)	36.2	26.5
(3)	$Xe_nEF_2^+ \rightarrow nXe + E^+ + F_2$					
B	288.8 (271.3)	285.8	272.1	294.5 (275.8)	291.6	271.6
Al	208.2 (195.6)	207.1	194.7	226.4 (213.6)	225.0	205.6
Ga	141.7 (129.7)	141.0	128.3	159.0 (146.7)	158.0	138.7
In	94.6 (87.9)	94.1	82.3	110.3 (102.8)	109.6	91.3
Tl	36.9 (35.3)	36.5	24.3	49.5 (46.5)	48.8	30.8

[a] Dissociation energies calculated at the CCSD(T)/def2-TZVP level are shown in parentheses. [b] Computed at 273.15 K.

The relative stability of **1a** against Xe loss follows the trend Al > B ≅ Ga > In > Tl, with the Al-containing complex being more stable than even its boron analogue. This trend is supported by D_e calculated at the CCSD(T)/def2-TZVP level (values in parentheses in Table 1) and by ΔG values computed at higher temperatures (298 and 373 K; Table S6). Moreover, the estimated D_e for $XeBF_2^+$ (25.7 kcal mol^{-1}) agrees with the previously reported value of 27.7 kcal mol^{-1} at the CCSD(T) level.[25]

Nature of bonding

Given the predicted energetic viability of several species, we analyzed the nature of Xe–icosagen bonding using various theoretical approaches. First, an energy decomposition analysis (EDA), a method widely used to explore bonding in Ngs compounds,[83,84] was conducted. The MF_2^+ cation and the Xe atom(s) were selected as fragments, consistent with the most favorable dissociation channels. For **1a** (Fig. 2a), the overall bond energy (ΔE_{bond}) indicates stronger Xe–EF_2^+ interactions when E = B, Al, or Ga. The interaction energy (ΔE_{int}) decreases from B to Tl, with the orbital interaction term (ΔE_{oi}) being the dominant component (Table S7). Notably, the percentage contribution of ΔE_{oi} reveals the highest covalent character for the Xe–Al bond (92%), followed by Xe–B (89%) and Xe–Ga bonds (83%). Although the Pauli repulsion (ΔE_{Pauli}) is larger for the boron compound, it is compensated by the high ΔE_{oi} magnitude (Fig. 2b). Overall, EDA suggests that the bonding stability in **1a** follows the trend: B ≅ Al ≅ Ga > In > Tl. A similar pattern is found for the **2a** species. However, ΔE_{bond} reveals stronger Xe_2–E interactions for Al and Ga (Table S8 and Fig. S1), resulting in a revised stability trend: Al ≅ Ga > B ≅ In > Tl.

Natural population analysis (NPA) indicates a net electron transfer from Xe to the EF_2^+ fragment (Table 2). In both **1a** and **2a**, Xe and E atoms carry partial positive charges, while the F atoms are negatively charged. The Xe atomic charge decreases from B to Tl, suggesting reduced charge transfer in the heavier analogues. Consistently, WBI values for the Xe–E bond range from 0.74–0.44 (B, Al, and Ga) to 0.34–0.24 (In and Tl). In particular, the relatively high WBI in $XeBF_2^+$ supports a strong covalent Xe–B interaction, in agreement with previous findings of Lv *et al.*[25] These results confirm that the Xe–E bond strength decreases along the series from B to Tl.

The AdNDP analysis further corroborates these findings. For the B, Al, and Ga species, a localized two-center, two-electron (2c-2e) Xe–E σ-bond is found, with an ideal occupation number (ON) of 2.00|e| (Fig. 3a). In contrast, no such bonding is present in the In and Tl species; instead, a 1c-2e lone pair is localized on the Xe atom, with ON values ranging from 1.82 to 1.87|e| (Fig. 3b). These results confirm that 2c-2e σ-bonding occurs only for the lighter elements, emphasizing a clear bonding distinction between B, Al, Ga, and their heavier congeners. A complete set of AdNDP analyses is provided in Fig. S2–S5.

To further investigate the electronic structure, we employed the localized orbital locator (LOL) and electron localization function (ELF), both derived from kinetic energy density. In these scalar fields, high values of $\eta(r)$ or $\nu(r)$ typically indicate covalent bonds, lone pairs, or core electron regions.[67–72]

Open Access Article. Published on 01 December 2025. Downloaded on 5/2/2026 7:54:11 AM.
This article is licensed under a Creative Commons Attribution 3.0 Unported Licence.

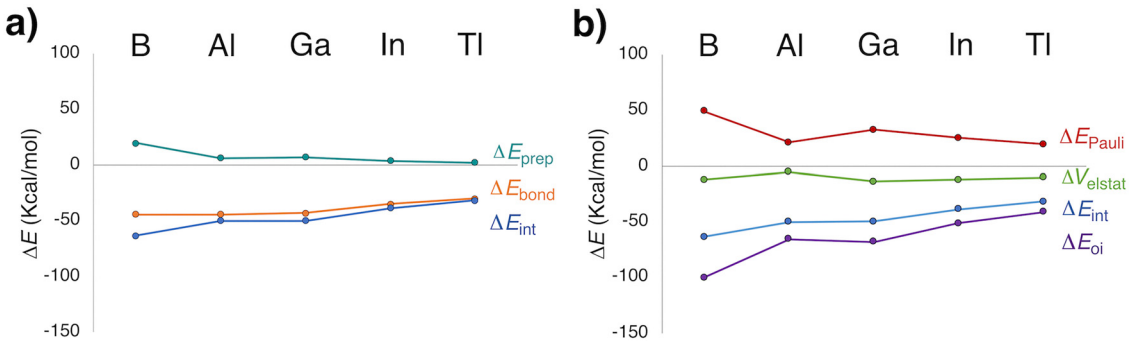

Fig. 2 (a) Decomposition of the bonding energy upon formation of $XeEF_2^+$ (**1a**) from the EF_2^+ and Xe fragments. (b) Energy decomposition analysis (EDA) of the interaction between EF_2^+ and Xe in the C_{2v} geometry adopted in **1a**.

Table 2 Wiberg bond indices for Xe–E and E–F bonds, and NPA charges (q, in $|e|$), calculated at the MP2/def2-TZVP level

	$XeEF_2^+$ (**1a**)					$Xe_2EF_2^+$ (**1b**)				
	WBI_{Xe-E}	WBI_{E-F}	q_{Xe}	q_E	q_F	WBI_{Xe-E}	WBI_{E-F}	q_{Xe}	q_E	q_F
B	0.735	0.874	0.503	1.449	−0.476	0.514	0.797	0.339	1.358	−0.518
Al	0.455	0.422	0.264	2.279	−0.771	0.422	0.405	0.246	2.062	−0.777
Ga	0.442	0.472	0.262	2.201	−0.732	0.424	0.429	0.253	2.001	−0.754
In	0.337	0.425	0.194	2.317	−0.756	0.352	0.400	0.204	2.131	−0.770
Tl	0.244	0.524	0.141	2.182	−0.661	0.263	0.503	0.153	2.053	−0.679

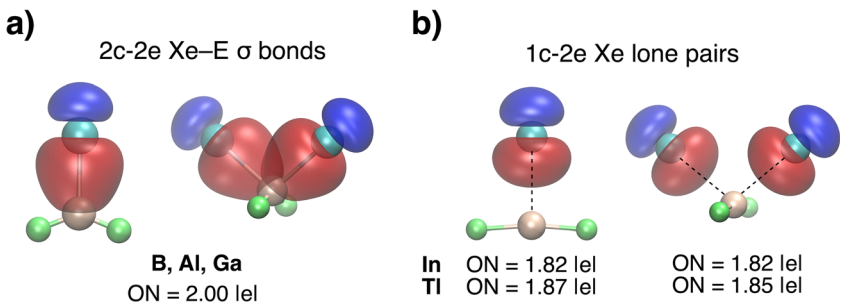

Fig. 3 AdNDP orbitals and occupation numbers (ON) for $XeEF_2^+$ (**1a**) and $Xe_2EF_2^+$ (**2a**): (a) localized 2c-2e Xe–E σ-bonds (E = B, Al, Ga); (b) 1c-2e lone pairs on Xe for In and Tl.

The 2D LOL and ELF plots for **1a** and **2a** show an increasing polarization of the Xe–E bond toward Xe from B to Tl (Fig. S6). This trend is especially apparent when comparing the bonding regions of the B and Tl species. As shown in Fig. 4, the Xe–B bond exhibits the most localized bonding region, consistent with its higher covalent character. These observations align well with the conclusions drawn from both AdNDP analysis and EDA.

NCI analysis[65,66] was performed to identify potential weak interactions. In the B-containing species, the isosurface maps display a blue region between Xe and B, while $Xe_2BF_2^+$ exhibits a small green region between the Xe atoms (Fig. S7 and S8). However, the absence of $(\lambda_2)\rho$ peaks in the −0.05 to 0.05 a.u. range confirms a lack of significant non-covalent interactions in these systems. In contrast, the Al and Ga species show blue isosurfaces and corresponding negative $(\lambda_2)\rho$ peaks, indicative of attractive non-covalent interactions. These features are even more pronounced in the In and Tl species, as shown in Fig. 5, with deeper blue regions and more negative $(\lambda_2)\rho$ values.

Overall, these findings are consistent with the bonding patterns established by EDA, NPA, WBI, and AdNDP: while a covalent Xe–B interaction dominates in the lighter species, non-covalent interactions increasingly contribute to the bonding in the heavier In and Tl compounds.

Lewis acidity

Given the preceding findings, a key question arises: what makes the Xe–icosagen interactions strong enough to stabilize these compounds and render them viable for experimental detection? A plausible explanation lies in the pronounced Lewis acidity of the EF_2^+ cations (E = B–Tl). A reliable metric of Lewis acidity is the fluoride ion affinity (FIA), defined as the negative

 This journal is © the Owner Societies 2026

Open Access Article. Published on 01 December 2025. Downloaded on 5/2/2026 7:54:11 AM.
This article is licensed under a Creative Commons Attribution 3.0 Unported Licence.

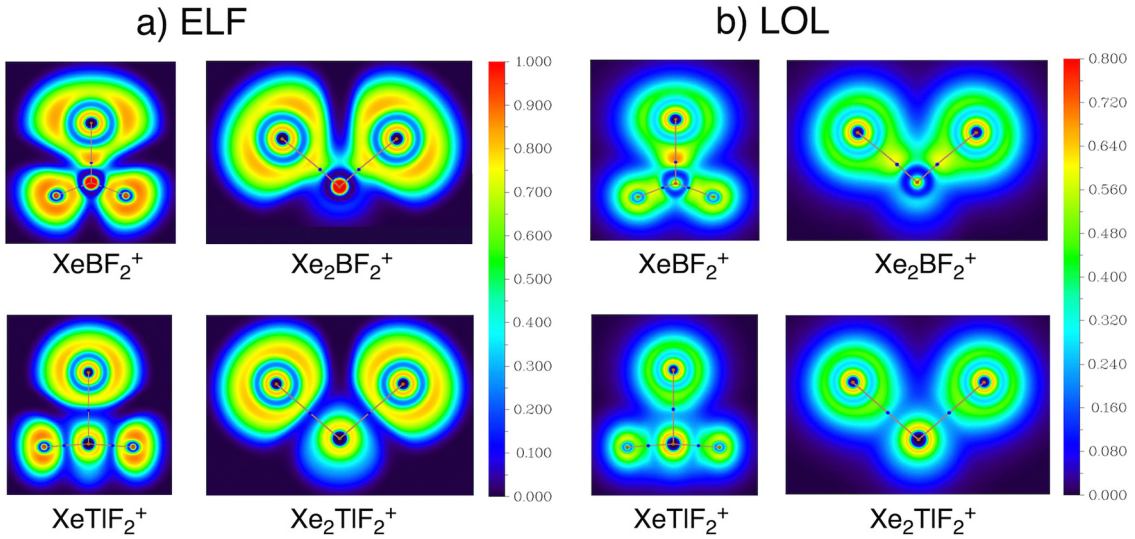

Fig. 4 Bonding analysis for $XeEF_2^+$ and $Xe_2EF_2^+$ (E = B and Tl) based on (a) electron localized function (ELF) and (b) localized orbital locator (LOL) maps.

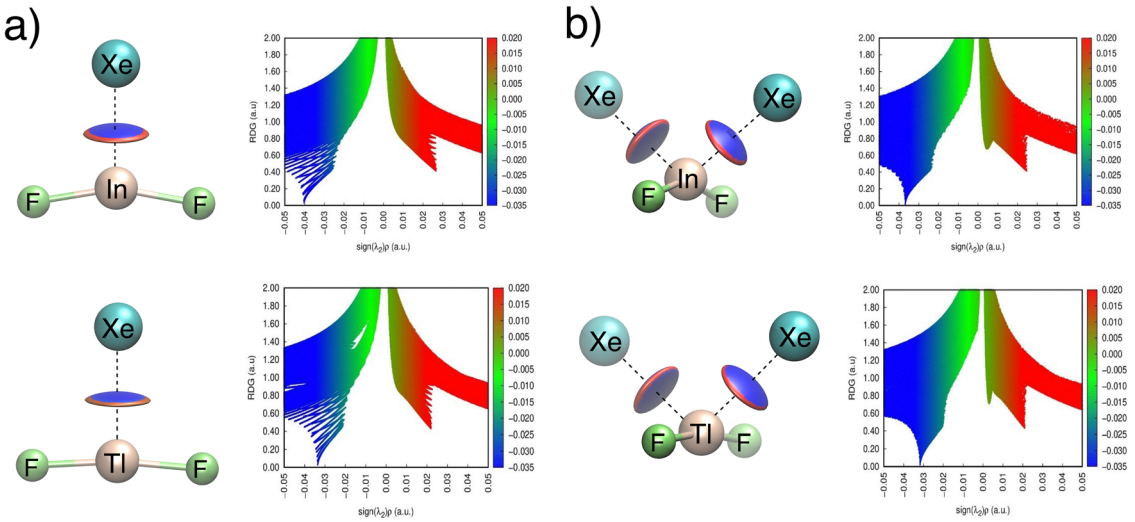

Fig. 5 Non-covalent interaction (NCI) isosurfaces and $(\lambda_2)\rho$ plots for (a) $XeEF_2^+$ and (b) $Xe_2EF_2^+$ species with E = In and Tl.

Table 3 Fluoride ion affinity (FIA, in kcal mol^{-1}) and A–F bond lengths (in Å) for A^+ species, computed at the CCSD(T)/def2-TZVPP level

A^+	FIA	A–F
$B(C_6F_5)_2^+$	250.2	1.3224
BH_2^+	297.3	1.3226
BF_2^+	349.9	1.3145
AlF_2^+	310.0	1.6325
GaF_2^+	293.7	1.7239
InF_2^+	266.3	1.9173
TlF_2^+	248.1	1.9924

enthalpy of the gas-phase reaction between a fluoride ion and a Lewis acid.[85] The computed FIA values for the EF_2^+ cations are summarized in Table 3. Higher FIA values indicate stronger Lewis acidity. For comparison, typical p-block Lewis acids exhibit FIA values in the range of 119.5–148.9 kcal mol^{-1}.[86] Notably, all EF_2^+ cations analyzed here exceed this range, with BF_2^+ and AlF_2^+ displaying even greater Lewis acidity than several well-known strong acids such as $B(C_6F_5)_2^+$ and BH_2^+.

The acidity trend follows the order: $BF_2^+ > AlF_2^+ > GaF_2^+ > InF_2^+ > TlF_2^+$. This strong electron-withdrawing character facilitates interaction with Xe, thereby stabilizing the Xe–icosagen bond. Consequently, beyond the previously reported $XeBF_2^+$ species, other Xe–icosagen compounds such as $XeAlF_2^+$ and $XeGaF_2^+$, which also show significant thermodynamic and kinetic stability, emerge as promising candidates for experimental detection.

^{129}Xe NMR chemical shift calculations

Given the high sensitivity of ^{129}Xe NMR to its chemical environment, the prediction of chemical shifts provides an additional probe for the Xe-icosagen interactions. To this end, we performed relativistic ^{129}Xe NMR chemical shift calculations in the

Open Access Article. Published on 01 December 2025. Downloaded on 5/2/2026 7:54:11 AM.
This article is licensed under a Creative Commons Attribution 3.0 Unported Licence.

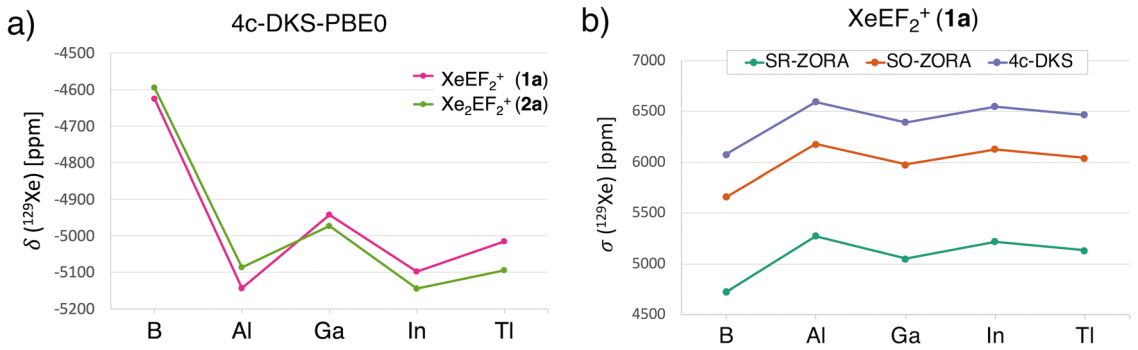

Fig. 6 (a) Predicted ^{129}Xe NMR chemical shifts (δ) for $XeEF_2^+$ (**1a**) and $Xe_2EF_2^+$ (**2a**) using the 4c-DKS-PBE0 method. (b) ^{129}Xe NMR shielding constants (σ) for **1a** computed with SR-ZORA, SO-ZORA, and 4c-DKS methods at the PBE0 level.

gas phase (see the Computational methods for details). The predicted ^{129}Xe NMR chemical shifts (δ) for the **1a** and **2a** species range from −5145 to −4600 ppm (Fig. 6a), significantly more shielded than those reported for the most upfield-shifted cationic Xe environments observed experimentally, such as in XeL^+ cations: $C_6F_5Xe^+$ (−3967.5 ppm),[87] $F_5TeN(H)Xe^+$ (*ca.* −2900 ppm),[88] $F_5SN(H)Xe^+$ (−2886 ppm),[89] and $F_4S{=}NXe^+$ (−2672 ppm).[90] In these species, polarization and relativistic effects distort the electron cloud, enhancing shielding and leading to strongly upfield shifts.

The more negative ^{129}Xe NMR chemical shifts predicted for **1a** and **2a** suggest that the EF_2^+ fragments induce greater polarization in Xe, promoting stronger covalent interactions. Among the series, $XeBF_2^+$ and $Xe_2BF_2^+$ are ∼300 ppm less shielded than their heavier analogues (Fig. 6a). This trend suggests that Xe–E bonding in the Al–Tl species possesses greater covalent character. Notably, the **1a** species with AlF_2^+ exhibits the most negative δ value (−5144 ppm), indicating the highest shielding. In the **2a** series, however, AlF_2^+ is slightly less shielded, allowing InF_2^+ to exhibit the most upfield shift.

To further assess the influence of relativistic effects, especially important for heavier atoms, we compared three computational approaches: the scalar relativistic (SR) ZORA approximation, the two-component spin–orbit (SO) ZORA, and the fully four-component Dirac–Kohn–Sham (4c-DKS) method based on the Dirac–Coulomb Hamiltonian. The calculated ^{129}Xe NMR shielding constants (σ) for **1a** and **2a** are shown in Fig. 6b and Fig. S9, respectively. At the SR-ZORA level, $\sigma(^{129}Xe)$ values for **1a** range from 4724 to 5276 ppm (green line, Fig. 6b). Inclusion of SO effects *via* the 2c-ZORA method increases shielding by ∼900 ppm, while the 4c-DKS approach yields an additional ∼400 ppm increase. Although the 4c-DKS method does not alter the trend from B to Tl, it significantly enhances overall shielding values. These results underscore the critical role of relativistic effects, particularly spin–orbit coupling, in accurately modeling ^{129}Xe NMR chemical shifts in Xe–icosagen species.

Conclusions

This study presents the first comprehensive analysis of Xe–icosagen interactions by examining the global minima of the $XeEF_2^+$ (**1a**) and $Xe_2EF_2^+$ (**2a**) cations (E = B–Tl), explicitly including the heavier icosagens In and Tl. Our computational results show that these species are both thermodynamically and kinetically stable in the gas phase, making them viable candidates for experimental detection. The most favorable dissociation pathway involves Xe loss and is consistently endothermic and endergonic across the series, highlighting the robustness of Xe–EF_2^+ bonding.

Energy Decomposition Analysis (EDA) indicates that the Xe–E bond stability in **1a** follows the trend B ≅ Al ≅ Ga > In > Tl, with comparable bonding strength among B, Al, and Ga. For the **2a** series, the trend shifts to Al ≅ Ga > B > In > Tl, where Al and Ga species exhibit even greater stability than their boron analogues. In both **1a** and **2a**, orbital interactions (ΔE_{oi}) dominate the bonding, with the highest covalent character observed for the Xe–Al bond.

AdNDP analysis confirms the presence of a 2c-2e σ-bond between Xe and E for the lighter elements (B, Al, and Ga), while only lone-pair character was found for In and Tl. This covalent-to-noncovalent transition is further supported by LOL and ELF descriptors, which reveal increasing polarization of the Xe–E bond and a gradual decline in covalent character down the group.

The EF_2^+ cations exhibit exceptionally high Lewis acidity, with FIA values surpassing those of well-known p-block Lewis acids. This strong electron-withdrawing capacity promotes Xe coordination and significantly contributes to complex stabilization.

Relativistic ^{129}Xe NMR chemical shift calculations reveal highly negative σ values, indicative of strong shielding and consistent with covalent Xe–E interactions. The inclusion of relativistic effects, particularly spin–orbit coupling, is crucial for accurately reproducing these NMR parameters.

In summary, Xe can form energetically stable and potentially covalent bonds with a broad range of icosagens, including heavier elements such as Al and Ga. The combination of high Lewis acidity, favorable thermodynamics, and distinctive ^{129}Xe NMR signatures identifies compounds like $XeAlF_2^+$ and $XeGaF_2^+$, alongside $XeBF_2^+$, as promising targets for experimental observation.

Conflicts of interest

There are no conflicts to declare.

This journal is © the Owner Societies 2026

Open Access Article. Published on 01 December 2025. Downloaded on 5/2/2026 7:54:11 AM. This article is licensed under a Creative Commons Attribution 3.0 Unported Licence.

Data availability

All computational data are available in the ioChem-BD repository and can be accessed *via* **https://doi.org/10.19061/iochem-bd-6-567**. Researchers and interested parties can access the dataset to facilitate further research and validation of the findings presented in this study.

Additional tables, figures and plots have been included as part of the supplementary information (SI). See DOI: **https://doi.org/10.1039/d5cp03397g**.

Acknowledgements

E. C. acknowledges the support provided by the Kukulcan Computing Center of Cinvestav Mérida. J. A. G.-C. and A. C. C. acknowledge the support from the Norwegian Research Council (grant no. 325231 and Centre of Excellence grant no. 262695) and the Norwegian Metacenter for Computational Science (NOTUR) through a grant of computer time (nn4654k). J. O. C. J.-H. acknowledges the Supercomputer Centre of the University of Guanajuato.

References

1 N. Bartlett, Xenon hexafluoroplatinate(V), Xe $[PtF_6]$, *Proc. Chem. Soc.*, 1962, 218.
2 R. Hoppe, W. Dähne, H. Mattauch and K. Rödder, Fluorination of Xenon, *Angew. Chem., Int. Ed. Engl.*, 1962, **1**(11), 599.
3 H. H. Claassen, H. Selig and J. G. Malm, Xenon Tetrafluoride, *J. Am. Chem. Soc.*, 1962, **84**(18), 3593.
4 W. Grochala, Atypical compounds of gases, which have been called 'noble', *Chem. Soc. Rev.*, 2007, **36**(10), 1632–1655.
5 F. Grandinetti, Gas-phase ion chemistry of the noble gases: recent advances and future perspectives, *Eur. J. Mass Spectrom.*, 2011, **17**(5), 423–463.
6 F. Grandinetti, *Noble Gas Chemistry: Structure, Bonding, and Gas-Phase Chemistry*, John Wiley & Sons, 2018.
7 R. Saha, G. Jana, S. Pan, G. Merino and P. K. Chattaraj, How Far Can One Push the Noble Gases Towards Bonding?: A Personal Account, *Molecules*, 2019, **24**, 2933.
8 S. Pan, G. Merino and P. K. Chattaraj, Editorial: ''Changing the Perspective of the Noble Gas Reactivity'', *Front. Chem.*, 2021, **9**, 658318.
9 L. Khriachtchev, M. Pettersson, N. Runeberg, J. Lundell and M. Rasanen, A stable argon compound, *Nature*, 2000, **406**(6798), 874–876.
10 X. Dong, A. R. Oganov, A. F. Goncharov, E. Stavrou, S. Lobanov, G. Saleh, G.-R. Qian, Q. Zhu, C. Gatti and V. L. Deringer, A stable compound of helium and sodium at high pressure, *Nat. Chem.*, 2017, **9**(5), 440–445.
11 A. Sirohiwal, D. Manna, A. Ghosh, T. Jayasekharan and T. K. Ghanty, Theoretical Prediction of Rare Gas Containing Hydride Cations: HRgBF(+) (Rg = He, Ar, Kr, and Xe), *J. Phys. Chem. A*, 2013, **117**(41), 10772–10782.
12 A. Ghosh, S. Dey, D. Manna and T. K. Ghanty, Noble-Gas-Inserted Fluoro(sulphido)boron (FNgBS, Ng = Ar, Kr, and Xe): A Theoretical Prediction, *J. Phys. Chem. A*, 2015, **119**(22), 5732–5741.
13 Y. H. Huang, Z. Z. Li and A. Y. Li, Hexagonal boron-noble gas compounds B(6)Ng(n)(4 +): Structures and bonding, *Chem. Phys. Lett.*, 2017, **689**, 82–91.
14 J. Y. Jin, W. Li, Y. H. Liu, G. J. Wang and M. F. Zhou, Preparation and characterization of chemically bonded argon-boroxol ring cation complexes, *Chem. Sci.*, 2017, **8**(9), 6594–6600.
15 M. Rohdenburg, M. Mayer, M. Grellmann, C. Jenne, T. Borrmann, F. Kleemiss, V. A. Azov, K. R. Asmis, S. Grabowsky and J. Warneke, Superelectrophilic Behavior of an Anion Demonstrated by the Spontaneous Binding of Noble Gases to $B_{12}Cl_{11}$(-), *Angew. Chem., Int. Ed.*, 2017, **56**(27), 7980–7985.
16 Z. Tan and A. Y. Li, Noble gas supported boron-pentagonal clusters $B_5Ng_n^{3+}$: exploring the structures and bonding, *J. Mol. Model.*, 2018, **24**(4), 1–12.
17 Z. Z. Li, M. Wen and A. Y. Li, Rg(n)Be(3)B(3)(+): theoretical investigation of $Be_3B_3^+$ and its rare gas capability, *J. Mol. Model.*, 2019, **25**(12), 12.
18 Z. Huang, Y. Guo and Y. Li, The bonds and aromaticities of $[NgB_xO_y]^+$(Ng = Ar, Kr and Xe; x = 3–5, y = 5–7), *Comput. Theor. Chem.*, 2020, 112798.
19 M. Mayer, M. Rohdenburg, V. van Lessen, M. C. Nierstenhöfer, E. Aprà, S. Grabowsky, K. R. Asmis, C. Jenne and J. Warneke, First steps towards a stable neon compound: Observation and bonding analysis of $[B_{12}(CN)_{11}Ne]^-$, *Chem. Commun.*, 2020, **56**(33), 4591–4594.
20 S. P. Kuntar, A. Ghosh and T. K. Ghanty, Superstrong Chemical Bonding of Noble Gases with Oxidoboron (BO^+) and Sulfidoboron (BS^+), *J. Phys. Chem. A*, 2022, **126**(43), 7888–7900.
21 R. P. Rios, A. Vásquez-Espinal, S. Pan, E. Cerpa, W. Tiznado and G. Merino, BH_4Ng^+ (Ar–Rn): Viable Compounds with a B-Ng Covalent Bond, *ChemPhysChem*, 2022, e202200601.
22 D. H. Tan, S. Y. Xian and A. Y. Li, Substituent Effects of Structures and Bonds of Noble Gas Compounds F–Rg–BR_2 (Rg= Ar, Kr, Xe, and Rn; R= F, OH, CN, and CCH), *Russian J. Phys. Chem. A*, 2022, **96**(3), 611–623.
23 S. P. Kuntar, A. Ghosh and T. K. Ghanty, Theoretical prediction of donor–acceptor type novel complexes with strong noble gas–boron covalent bond, *Phys. Chem. Chem. Phys.*, 2024, **26**(6), 4975–4988.
24 G. Wang, Q. Ma, B. Wang, Y. Yang, L. Zhao, M. Zhou and G. Frenking, Spectroscopy and Bonding Analysis of ArnBO+ (n = 1–3) Cations That Possess Argon–Boron Multiple Bonds, *J. Am. Chem. Soc.*, 2025, **147**(3), 2491–2501.
25 Z. Lv, G. H. Chen, D. Li, D. Wu, X. C. Huang, Z. R. Li and W. G. Liu, RgBF(2)(+) complexes (Rg = Ar, Kr, and Xe): The cations with large stabilities, *J. Chem. Phys.*, 2011, **134**(15), 154302.
26 L. Arrué and R. Pino-Rios, Boron–noble gas covalent bonds in borenium and boronium compounds, *Phys. Chem. Chem. Phys.*, 2021, **23**(11), 6896–6902.
27 A. M. Gardner, K. A. Gutsmiedl, T. G. Wright, W. Breckenridge, C. Y. Chapman and L. A. Viehland, Theoretical study

Open Access Article. Published on 01 December 2025. Downloaded on 5/2/2026 7:54:11 AM. This article is licensed under a Creative Commons Attribution 3.0 Unported Licence.

of Al^+–RG (RG= He–Rn), *J. Chem. Phys.*, 2010, **133**(16), 164302.
28 A. M. Gardner, K. A. Gutsmiedl, T. G. Wright, E. P. F. Lee, W. H. Breckenridge, S. Rajbhandari, C. Y. N. Chapman and L. A. Viehland, Theoretical Study of M^+—RG Complexes (M = Ga, In; RG = He—Rn), *J. Phys. Chem. A*, 2011, **115**(25), 6979–6985.
29 T. Jayasekharan and T. K. Ghanty, Insertion of rare gas atoms into BF_3 and AlF_3 molecules: An ab initio investigation, *J. Chem. Phys.*, 2006, **125**(23), 234106.
30 A. Ghosh, A. Mallick and T. K. Ghanty, Anomaly in the stability of the hydroxides of icosagens (B and Al) and their noble gas (Xe and Rn) derivatives: a comparative study, *Phys. Chem. Chem. Phys.*, 2020, **22**(25), 14109–14124.
31 L. A. Mück, A. Y. Timoshkin, M. V. Hopffgarten and G. Frenking, Donor acceptor complexes of noble gases, *J. Am. Chem. Soc.*, 2009, **131**(11), 3942–3949.
32 E. Makarewicz, A. J. Gordon and S. Berski, The electronic structure of the xenon insertion compounds XXe–MX_2 (X = F, Cl, Br, I; M = B, Al, Ga), *Polyhedron*, 2016, **117**, 97–109.
33 J. Haner and G. J. Schrobilgen, The Chemistry of Xenon(IV), *Chem. Rev.*, 2015, **115**(2), 1255–1295.
34 D. Raftery, Xenon NMR Spectroscopy, in *Annual Reports on NMR Spectroscopy*, ed. Webb, G. A., Academic Press, vol. 57, 2006, pp. 205–270.
35 A. Bagno and G. Saielli, DFT Study of the NMR Properties of Xenon in Covalent Compounds and van der Waals Complexes—Implications for the Use of ^{129}Xe as a Molecular Probe, *Chem. – Eur. J.*, 2003, **9**(7), 1486–1495.
36 M. Gerken and G. J. Schrobilgen, The impact of multi-NMR spectroscopy on the development of noble-gas chemistry, *Coord. Chem. Rev.*, 2000, **197**(1), 335–395.
37 P. Lantto and J. Vaara, Xe^{129} chemical shift by the perturbational relativistic method: Xenon fluorides, *J. Chem. Phys.*, 2007, **127**(8), 084312.
38 M. Straka, P. Lantto and J. Vaara, Toward Calculations of the ^{129}Xe Chemical Shift in Xe@C_{60} at Experimental Conditions: Relativity, Correlation, and Dynamics, *J. Phys. Chem. A*, 2008, **112**(12), 2658–2668.
39 S. Standara, P. Kulhánek, R. Marek, J. Horníček, P. Bouř and M. Straka, Simulations of ^{129}Xe NMR chemical shift of atomic xenon dissolved in liquid benzene, *Theor. Chem. Acc.*, 2011, **129**(3), 677–684.
40 P. Lantto, S. Kangasvieri and J. Vaara, Rovibrational effects on NMR shieldings in a heavy-element system: XeF_2, *J. Chem. Phys.*, 2012, **137**(21), 214309.
41 P. Lantto, S. Standara, S. Riedel, J. Vaara and M. Straka, Exploring new ^{129}Xe chemical shift ranges in HXeY compounds: hydrogen more relativistic than xenon, *Phys. Chem. Chem. Phys.*, 2012, **14**(31), 10944–10952.
42 M. A. Gonçalves, G. A. Andolpho, E. F. F. da Cunha and T. C. Ramalho, Exploring ^{129}Xe NMR parameters for structural investigation of biomolecules: relativistic, solvent, and thermal effects, *J. Mol. Model.*, 2022, **28**(11), 372.
43 J. L. Cabellos, F. Ortiz-Chi, A. Ramirez and G. Merino, *GLOMOS 1.0*, Cinvestav Merida, Yuc. Mexico, 2013.
44 C. Adamo and V. Barone, Toward reliable density functional methods without adjustable parameters: The PBE0 model, *J. Chem. Phys.*, 1999, **110**(13), 6158–6170.
45 F. Weigend and R. Ahlrichs, Balanced basis sets of split valence, triple zeta valence and quadruple zeta valence quality for H to Rn: Design and assessment of accuracy, *Phys. Chem. Chem. Phys.*, 2005, **7**(18), 3297–3305.
46 B. Metz, M. Schweizer, H. Stoll, M. Dolg and W. Liu, A small-core multiconfiguration Dirac–Hartree–Fock-adjusted pseudopotential for Tl–application to Tl X (X= F, Cl, Br, I), *Theor. Chem. Acc.*, 2000, **104**(1), 22–28.
47 B. Metz, H. Stoll and M. Dolg, Small-core multiconfiguration-Dirac–Hartree–Fock-adjusted pseudopotentials for post-d main group elements: Application to PbH and PbO, *J. Chem. Phys.*, 2000, **113**(7), 2563–2569.
48 K. A. Peterson, D. Figgen, E. Goll, H. Stoll and M. Dolg, Systematically convergent basis sets with relativistic pseudopotentials. II. Small-core pseudopotentials and correlation consistent basis sets for the post-d group 16–18 elements, *J. Chem. Phys.*, 2003, **119**(21), 11113–11123.
49 M. Frisch, G. Trucks, H. Schlegel, G. Scuseria, M. Robb, J. Cheeseman, G. Scalmani, V. Barone, G. Petersson and H. Nakatsuji, *Gaussian 16*, Gaussian, Inc., Wallingford, CT, 2016.
50 K. Morokuma, Why do molecules interact? The origin of electron donor-acceptor complexes, hydrogen bonding and proton affinity, *Acc. Chem. Res.*, 1977, **10**(8), 294–300.
51 T. Ziegler and A. Rauk, On the Calculation of Bonding Energies by the Hartree Fock Slater Method, *Theor. Chim. Acta*, 1977, **46**, 1–10.
52 F. M. Bickelhaupt and E. J. Baerends, Kohn-Sham density functional theory: predicting and understanding chemistry, *Rev. Comput. Chem.*, 2000, **15**, 1–86.
53 J. P. Perdew, Density-functional approximation for the correlation energy of the inhomogeneous electron gas, *Phys. Rev. B: Condens. Matter Mater. Phys.*, 1986, **33**(12), 8822–8824.
54 A. D. Becke, Density-functional exchange-energy approximation with correct asymptotic behavior, *Phys. Rev. A: At., Mol., Opt. Phys.*, 1988, **38**(6), 3098–3100.
55 S. Grimme, J. Antony, S. Ehrlich and H. Krieg, A consistent and accurate ab initio parametrization of density functional dispersion correction (DFT-D) for the 94 elements H-Pu, *J. Chem. Phys.*, 2010, **132**(15), 154104.
56 S. Grimme, S. Ehrlich and L. Goerigk, Effect of the Damping Function in Dispersion Corrected Density Functional Theory, *J. Comput. Chem.*, 2011, **32**(7), 1456–1465.
57 E. van Lenthe, E. J. Baerends and J. G. Snijders, Relativistic regular 2-component hamiltonians, *J. Chem. Phys.*, 1993, **99**(6), 4597–4610.
58 E. van Lenthe, E. J. Baerends and J. G. Snijders, Relativistic total-energy using regular approximations, *J. Chem. Phys.*, 1994, **101**(11), 9783–9792.
59 E. van Lenthe, R. van Leeuwen, E. J. Baerends and J. G. Snijders, Relativistic regular two-component Hamiltonians, *Int. J. Quantum Chem.*, 1996, **57**(3), 281–293.

Open Access Article. Published on 01 December 2025. Downloaded on 5/2/2026 7:54:11 AM. This article is licensed under a Creative Commons Attribution 3.0 Unported Licence.

60 E. van Lenthe, J. G. Snijders and E. J. Baerends, The zero-order regular approximation for relativistic effects: The effect of spin-orbit coupling in closed shell molecules, *J. Chem. Phys.*, 1996, **105**(15), 6505–6516.
61 E. van Lenthe, A. Ehlers and E. J. Baerends, Geometry optimizations in the zero order regular approximation for relativistic effects, *J. Chem. Phys.*, 1999, **110**(18), 8943–8953.
62 G. te Velde, F. M. Bickelhaupt, E. J. Baerends, C. F. Guerra, S. J. A. Van Gisbergen, J. G. Snijders and T. Ziegler, Chemistry with ADF, *J. Comput. Chem.*, 2001, **22**(9), 931–967.
63 D. Y. Zubarev and A. I. Boldyrev, Developing paradigms of chemical bonding: adaptive natural density partitioning, *Phys. Chem. Chem. Phys.*, 2008, **10**(34), 5207–5217.
64 D. Y. Zubarev and A. I. Boldyrev, Revealing Intuitively Assessable Chemical Bonding Patterns in Organic Aromatic Molecules via Adaptive Natural Density Partitioning, *J. Org. Chem.*, 2008, **73**(23), 9251–9258.
65 E. R. Johnson, S. Keinan, P. Mori-Sánchez, J. Contreras-García, A. J. Cohen and W. Yang, Revealing Noncovalent Interactions, *J. Am. Chem. Soc.*, 2010, **132**(18), 6498–6506.
66 J. Contreras-García, E. R. Johnson, S. Keinan, R. Chaudret, J.-P. Piquemal, D. N. Beratan and W. Yang, NCIPLOT: A Program for Plotting Noncovalent Interaction Regions, *J. Chem. Theory Comput.*, 2011, **7**(3), 625–632.
67 A. D. Becke and K. E. Edgecombe, A simple measure of electron localization in atomic and molecular-systems, *J. Chem. Phys.*, 1990, **92**(9), 5397–5403.
68 Y. Grin, A. Savin and B. Silvi, The ELF Perspective of chemical bonding, in *Chemical Bond: Fundamental Aspects of Chemical Bonding*, ed. G. Frenking and S. Shaik, Wiley-VCH Verlag GmbH, 2014, pp. 345–382.
69 H. Jacobsen, Localized-orbital locator (LOL) profiles of chemical bonding, *Can. J. Chem.*, 2008, **86**(7), 695–702.
70 H. Jacobsen, Chemical Bonding in View of Electron Charge Density and Kinetic Energy Density Descriptors, *J. Comput. Chem.*, 2009, **30**(7), 1093–1102.
71 H. Jacobsen, Localized-orbital locator (LOL) profiles of transition-metal hydride and dihydrogen complexes(1,2), *Can. J. Chem.*, 2009, **87**(7), 965–973.
72 H. Jacobsen, Topology maps of bond descriptors based on the kinetic energy density and the essence of chemical bonding, *Phys. Chem. Chem. Phys.*, 2013, **15**(14), 5057–5066.
73 T. Lu and F. W. Chen, Multiwfn: A multifunctional wavefunction analyzer, *J. Comput. Chem.*, 2012, **33**(5), 580–592.
74 S. Komorovský, M. Repiský, O. L. Malkina, V. G. Malkin, I. Malkin Ondík and M. Kaupp, A fully relativistic method for calculation of nuclear magnetic shielding tensors with a restricted magnetically balanced basis in the framework of the matrix Dirac–Kohn–Sham equation, *J. Chem. Phys.*, 2008, **128**(10), 104101.
75 S. Komorovský, M. Repiský, O. L. Malkina and V. G. Malkin, Fully relativistic calculations of NMR shielding tensors using restricted magnetically balanced basis and gauge including atomic orbitals, *J. Chem. Phys.*, 2010, **132**(15), 154101.
76 M. Repisky, S. Komorovsky, M. Kadek, L. Konecny, U. Ekström, E. Malkin, M. Kaupp, K. Ruud, O. L. Malkina and V. G. Malkin, ReSpect: Relativistic spectroscopy DFT program package, *J. Chem. Phys.*, 2020, **152**(18), 184101.
77 K. G. Dyall, Relativistic double-zeta, triple-zeta, and quadruple-zeta basis sets for the 5d elements Hf–Hg, *Theor. Chem. Acc.*, 2004, **112**(5), 403–409.
78 Basis sets are available from the Dirac web site, **https://dirac.chem.sdu.dk**.
79 K. G. Dyall, Core correlating basis functions for elements 31–118, *Theor. Chem. Acc.*, 2012, **131**(5), 1217.
80 E. van Lenthe and E. J. Baerends, Optimized Slater-type basis sets for the elements 1–118, *J. Comput. Chem.*, 2003, **24**(9), 1142–1156.
81 R. Ditchfield, Self-consistent perturbation theory of diamagnetism, *Mol. Phys.*, 1974, **27**(4), 789–807.
82 M. Álvarez-Moreno, C. de Graaf, N. López, F. Maseras, J. M. Poblet and C. Bo, Managing the Computational Chemistry Big Data Problem: The ioChem-BD Platform, *J. Chem. Inf. Model.*, 2015, **55**(1), 95–103.
83 D. Chakraborty and P. K. Chattaraj, In quest of a superhalogen supported covalent bond involving a noble gas atom, *J. Phys. Chem. A*, 2015, **119**(12), 3064–3074.
84 S. Pan, A. Gupta, S. Mandal, D. Moreno, G. Merino and P. K. Chattaraj, Metastable behavior of noble gas inserted tin and lead fluorides, *Phys. Chem. Chem. Phys.*, 2015, **17**(2), 972–982.
85 K. O. Christe, D. A. Dixon, D. McLemore, W. W. Wilson, J. A. Sheehy and J. A. Boatz, On a quantitative scale for Lewis acidity and recent progress in polynitrogen chemistry, *J. Fluor. Chem.*, 2000, **101**(2), 151–153.
86 P. Erdmann, J. Leitner, J. Schwarz and L. Greb, An Extensive Set of Accurate Fluoride Ion Affinities for p-Block Element Lewis Acids and Basic Design Principles for Strong Fluoride Ion Acceptors, *ChemPhysChem*, 2020, **21**(10), 987–994.
87 H.-J. Frohn, A. Klose, T. Schroer, G. Henkel, V. Buss, D. Opitz and R. Vahrenhorst, Structural, Chemical, and Theoretical Evidence for the Electrophilicity of the $[C_6F_5Xe]^+$ Cation in $[C_6F_5Xe][AsF_6]$, *Inorg. Chem.*, 1998, **37**(19), 4884–4890.
88 B. Fir, J. M. Whalen, H. P. A. Mercier, D. A. Dixon and G. J. Schrobilgen, Syntheses of $[F_5TeNH_3][AsF_6]$, $[F_5TeN(H)Xe][AsF_6]$, and F_5TeNF_2 and Characterization by Multi-NMR and Raman Spectroscopy and by Electronic Structure Calculations: The X-ray Crystal Structures of α- and β-F_5TeNH_2, $[F_5TeNH_3][AsF_6]$, and $[F_5TeN(H)Xe][AsF_6]$, *Inorg. Chem.*, 2006, **45**(5), 1978–1996.
89 G. L. Smith, H. P. A. Mercier and G. J. Schrobilgen, $F_5SN(H)Xe^+$; a Rare Example of Xenon Bonded to sp3-Hybridized Nitrogen; Synthesis and Structural Characterization of $[F_5SN(H)Xe][AsF_6]$, *Inorg. Chem.*, 2008, **47**(10), 4173–4184.
90 G. L. Smith, H. P. A. Mercier and G. J. Schrobilgen, Solid-State and Solution Rearrangements of $F_3S \equiv NXeF^+$ Leading to the $F_4S{=}NXe^+$ Cation; Syntheses, HF Solvolyses, and Structural Characterizations of $[F_4S{=}NXe][AsF_6]$ and $[F_4S{=}NH_2][AsF_6]$, *J. Am. Chem. Soc.*, 2009, **131**(21), 7272–7286.